Numerical model using a Volume-Of-Fluid method for the study of evaporating sessile droplets in both unpinned and pinned modes

Cécile Lalanne, Quentin Magdelaine, Florence Lequien, José-Maria Fullana

Version of Record: https://www.sciencedirect.com/science/article/pii/S0997754621000881
Manuscript_e1fd23e5c178e04e1c1133962f75dde1

Numerical model using a Volume-Of-Fluid method for the study of evaporating sessile droplets in both unpinned and pinned modes

Cécile Lalanne[a,b,*], Quentin Magdelaine[b,c], Florence Lequien[a], José-Maria Fullana[b]

[a] *Université Paris-Saclay, CEA, Service de la Corrosion et du Comportement des Matériaux dans leur Environnement, 91191, Gif-sur-Yvette, France*
[b] *Sorbonne Université, CNRS, UMR 7190, Institut Jean Le Rond d'Alembert, Paris, France*
[c] *Surface du Verre et Interfaces, UMR 125 CNRS/Saint-Gobain, Aubervilliers, France*

Abstract

We propose a numerical study of the evaporation of sessile droplets using a Volume-Of-Fluid (VOF) method in the free-software Basilisk. We consider pure liquid droplets forming a spherical-cap onto a smooth or rough substrate and we investigate two different modes of evaporation: the unpinned mode where the contact angle is constant and the pinned mode where the wetting area is constant. The numerical method used to implement the contact angle and for the reconstruction of the interface is fully described, especially for the pinned mode for which we present a new VOF implementation. In the unpinned mode, the parametric studies predict that the volume decreases in time according two phases, which matches the signature behaviour of evaporating unpinned droplets, irrespective of the geometrical parameters. In the pinned mode, the volume follows a linear decrease for the whole evaporation time and the contact angle analysis indicates a linear decrease in time which was expected according to the theory and validated with some experiments we performed.

Keywords: sessile drop, evaporation, pinned, unpinned, Volume-Of-Fluid

*Corresponding author
Email address: cecile.lalanne@dalembert.upmc.fr (Cécile Lalanne)

1. Introduction

Evaporation of liquid drops in the air is a phenomenon of loss mass that appears when the air is not saturated with the vapor of the liquid: interest in this field has been driven by academic and industrial applications. Since Maxwell [1] and later Langmuir [2], who studied the simplest evaporation problem of a spherical drop and derived the general framework of the studies of drop evaporation in an infinite medium, lots of theoretical works have investigated the process of drying. In particular, drops containing dispersed particles [3, 4, 5] are considered because of their fundamental role in industrial applications such as metal corrosion [6], ink-jet printing [7] or patterning of substrates [8].

For a sessile drop deposited on a solid substrate, the evaporation dynamics is generally quasi-steady and controlled by a diffusion process of vapor into the air [1, 9, 10, 11, 12, 13] where the contact angle between the interface and the substrate at the intersection of the three-phase contact line, the diffusion coefficient of water vapor in air, and the external condition control the mass flux across the interface. Consequently, the drop mass decreases in time but the temporal dynamics of the contact area, the drop radius, and the contact angle depend on the behaviour of the contact line [9].

Evaporation occurs often following three principal modes [14]: unpinned, where the radius decreases; pinned, where the contact angle decreases; and stick-and-slide, where both the radius and the contact angle can vary independently. These modes usually follow one another during the whole evaporation but most of the time, only one mode predominates: thus, in our simulations, only one mode is considered during the entire evaporation. Each mode has a huge impact on the dynamics of flows inside the drop, especially for drops containing dispersed particles. Indeed, the spatial shape of the deposit, for instance the patterns of stain at the end of the process of evaporation, depends on the evaporation mode, on the particles concentration and is under control of the capillary flows inside the drop. A well-known example is the ring-shaped pattern called the coffee-ring [3]. The patterns are the key drivers in many engineering appli-

cations: for instance, for saline sessile drops, the local salt deposit at the end of evaporation can induce local surface reactions like corrosion [6]. The capillary flows are principally radial because of the tension surface and the spherical-cap shape of the drop: the resulting flows transport dispersed particles to the contact line. Consequently, the repartition of the solute particles along the interface becomes non-homogeneous and leads to surface tension gradients. This produces solutal Marangoni flows that may be directed either towards or away from the edge of the drop [15, 16, 17, 18].

The complete evaporation process is challenging to understand and a way to do it is to combine analytical and numerical approaches. In this communication, we investigate the evaporation of pure liquid droplets. In the case of pure liquid evaporation and in particular pure water evaporation, the heat transfert at the interface appears minor so we decided to neglect the thermal Marangoni effects [19]. Simulating a pure liquid droplet is simpler because we do not deal with particle transport, chemical species concentration, or pinning due to a particle deposit. But, it is an excellent model for trying approaches and for numerical tests. This work will be further completed to study mixture droplets with dispersed particles. We propose then to study numerically the evaporation dynamics of pure liquid droplets, with a free software called Basilisk [20], that implements numerical methods for partial differential equations such as Navier-Stokes. A Volume-Of-Fluid (VOF) method is used to describe the interface and to handle the moving contact line [21]. The implementation of the contact angle, in particular in the pinned mode with the no-slip boundary condition [22], represents an important numerical interest. The validity of the numerical approaches employed will be demonstrated by the confrontation against theories and experimental data [6, 9, 14, 23, 24]. The Section 2 presents briefly the theory of the droplet evaporation and in Section 3 we detail the numerical method used to investigate the two modes of evaporation. In particular, we give a complete description of the numerical implementation for the pinned mode in the framework of a VOF implementation. Section 4 presents the numerical results and for the pinned mode, a comparison with experiences we performed.

2. Analytical model for droplet evaporation

2.1. Spherical droplet

The first approach for the modeling of a spherical droplet evaporation was proposed by Maxwell [1] in 1877, who found an analytical solution with an electrostatics analogy. Later, Langmuir [2] proposed a heat conduction analogy to derive the same relation for the mass evaporation rate.

The evaporation phenomenon is a phase change transition from a liquid to its own vapor. A droplet of water evaporating into air at room temperature can be described, in a first approximation, as a diffusive mechanism where water vapor is transported into the gas phase [14]. Then, other supplementary heat and mass transfer mechanisms can appear, such as convection or radiation.

When a spherical droplet evaporates into air, the vapor concentration field is not uniform through the gas phase, but it is uniform along the interface. Indeed, the vapor concentration at the droplet surface equals to its equilibrium or saturation condition c_s, whereas, far from the droplet, the vapor concentration reaches the boundary value $c_\infty \approx Hc_s$, where H is the relative humidity of the environment. This vapor concentration difference in the surrounding gas phase creates a concentration gradient which drives the evaporation process. Therefore, evaporation can be described by a diffusion equation for the vapor concentration, c

$$\partial_t c = \nabla \cdot (D_v \nabla c) \tag{1}$$

where t is the time and D_v is the water vapor diffusivity in the air.

In our study, we consider small droplets that keep a spherical-cap shape during the whole process of evaporation. A droplet adopts a spherical shape if the gravity g can be neglected compared to the surface tension γ [14]. The ratio between surface and inertia forces defines the dimensionless Bond number, $Bo = (\Delta\rho g r_0 h_0)/\gamma$, where $\Delta\rho$ is the density difference between the liquid and the air, r_0 is the initial radius of the drop and h_0 is the initial height of the drop. This number has to be lower than 1 to have a spherical-cap.

A droplet evaporation is not a stationary process but it can be considered as

a quasi-steady process as long as the vapor concentration adjusts rapidly compared to the time required for the entire droplet evaporation, t_F. Therefore, the transient term, $\partial_t c$, can be neglected in Equation (1) which simplifies into the Laplace equation, $\Delta c = 0$. The vapor concentration field is thus the solution of a Laplace equation and the vapor transport is only a mass diffusion. For a spherical droplet in air, the outward evaporation mass flux $\mathbf{J}$ along the interface is described by the Fick's law

$$\mathbf{J}(r,t) = \mathbf{n} \,.\, D_v \nabla c \tag{2}$$

where r is the drop radius and $\mathbf{n}$ is the normal vector to the droplet surface. From the evaporation mass flux, an evaporation velocity, noted v_e, can be defined. This velocity determines the liquid mass that is transformed into vapor during the evaporation, $\rho_l v_e$, where ρ_l is the liquid density. According to the mass balance at the interface, we can write:

$$\begin{aligned} \rho_l v_e \approx D_v \nabla c \approx D_v \frac{(c_s - c_\infty)}{r_0} \\ v_e \approx \frac{D_v (c_s - c_\infty)}{\rho_l r_0} \end{aligned} \tag{3}$$

This velocity scale defines the dimensionless Peclet number $Pe \approx (v_e r_0)/D_v \approx c_s/\rho_l \approx cste$. Thus, Pe is a constant for the problem and is smaller than 1 (of the order of 10^{-5}) which indicates that the vapor diffusion process is faster than the droplet evaporation so that the hypothesis on the quasi-steady regime is consistent. Indeed, the diffusion time scale is $t_D = r_0^2/D_v$, with r_0 the typical length of the drop (the initial radius), so the time ratio appears very small:

$$\frac{t_D}{t_F} = \frac{r_0^2}{D_v t_F} \approx \frac{c_s - c_\infty}{\rho_l} \approx \frac{c_s(1-H)}{\rho_l} \ll 1 \tag{4}$$

For instance, the time ratio for water is between 10^{-6} and 10^{-9}, depending on the surrounding air humidity [14].

2.2. Sessile droplet

Figure 1 shows a sessile droplet configuration where the presence of the substrate induces a loss of symmetry and the emergence of a triple contact

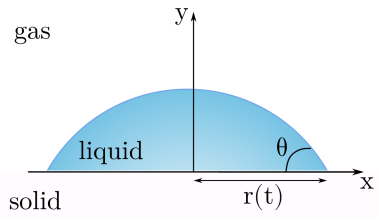

Figure 1: Sessile droplet sitting on a solid substrate. The interface of the drop forms a contact angle θ with the substrate surface.

point with solid, liquid, vapor in a singular point. Several authors [4, 9, 25] used the electrostatics analogy as Maxwell [1] did to derive a model for a sessile droplet evaporation. The evaporation mass flux along the drop interface is not uniform anymore because of the contact with the substrate. The analytical solutions for a sessile droplet are quite complex compared to the solution for a spherical droplet as long as they are dependent on the value of the contact angle, θ. Therefore, only approximated solutions for the evaporation mass flux profile $\mathbf{J}(r,t)$ exist as the one proposed by [26]. For a spherical-cap sessile droplet, the volume V can be expressed as

$$V(r,\theta) = \frac{\pi r^3}{3}\frac{(1-cos\theta)^2(2+cos\theta)}{sin^3\theta} \tag{5}$$

The total time of evaporation t_F can be predicted as [14]

$$t_F = \frac{\pi\rho r_0^2\theta_0}{16D_v\Delta c} \tag{6}$$

where θ_0 is the initial contact angle.

3. Numerical model

A sessile droplet is a three-phase problem, as the droplet is in contact with a solid substrate and with the gaseous environment. With appropriate boundary conditions and the implementation of an adjustable contact angle, we can simulate the action of the substrate on the droplet, and thus, we obtain a two-phase problem to solve numerically. The evaporation problem requires solving

the Navier-Stokes equations, the diffusion equation, and the advection of the interface.

3.1. Basilisk

We use a free software, Basilisk [20], based on the Gerris solver [27, 28] previously developed by the same authors, and benefits from various improvements as in particular the mesh adaptation methods. We solve a two-phase problem, with the one-fluid formulation: the different phases are treated as one fluid with variable material properties that change abruptly at the interface between the phases. We thus introduce the volume fraction $f(x,t)$, which equals to 1 for the liquid, index l, 0 for the surrounding air, index g and between 0 and 1 for the interface cells. We define the density and viscosity as functions of f, i.e. $\rho = f\rho_l + (1-f)\rho_g$ and $\mu = f\mu_l + (1-f)\mu_g$. The advection equation for the density can then be replaced with an equivalent advection equation for the volume fraction $\partial_t f + \boldsymbol{\nabla} \cdot (f\mathbf{u}) = 0$, where $\mathbf{u}$ is the velocity.

The spatial discretization is done using a quad-tree square cells structure in 2D (octree in 3D). It allows less costly dynamical grid refinement into user-defined regions which is really useful for two-phase flows as most of the interesting physics takes place in the vicinity of the interface (see Figure 2 for an example of adaptative discretization). This Adaptative Mesh Refinement (AMR) is one of the key strengths of Basilisk.

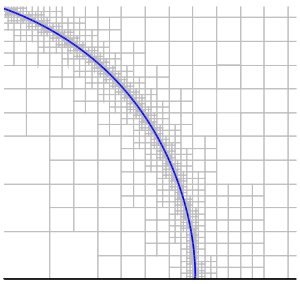

Figure 2: Example of the Adaptative Mesh Refinement (in grey) in Basilisk around an interface (in blue). The mesh automatically adjusts into user-defined regions to capture all the physics of the problem.

3.2. Navier-Stokes equations

Basilisk uses a finite volume approach which provides a conservative numerical scheme, thus the precision of the transport only depends on the scheme order and the mesh refinement. To solve the Navier-Stokes equations, as we consider an incompressible flow, we make use of the solver provided by Basilisk, based on a CFL-limited timestep, the Bell-Collela-Glaz advection scheme, and the implicit viscosity solver. We added the term representing the volume source arising from the phase-change. We detail here the time integration with the projection method, as the pressure plays a specific role for incompressible flows. A staggered in time discretization of the density and pressure leads to a formally second-order accurate time discretization

$$\frac{\mathbf{u}^{n+1}-\mathbf{u}^{n}}{\Delta t}+\mathbf{A}^{n}=\frac{1}{\rho_{n}}\left(-\nabla p+\mathbf{D}^{n}+\mathbf{f}^{n}\right) \tag{7}$$

where p is the pressure, $\mathbf{A}=\nabla\cdot(\mathbf{uu})$ is the advection term, $\mathbf{D}=\nabla\cdot\mu(\nabla\mathbf{u}+\nabla\mathbf{u}^{T})$ is the diffusion term and $\mathbf{f}$ denotes all other forces, such as gravity and surface tension. Then, the projection step computes an intermediate velocity field $\boldsymbol{u}^{*}$

$$\mathbf{u}^{*}=\mathbf{u}^{n}+\Delta t\left(-\mathbf{A}^{n}+\frac{1}{\rho^{n}}\left(\mathbf{D}^{n}+\mathbf{f}^{n}\right)\right) \tag{8}$$

The pressure is calculated such that the velocity at the new time step is divergence free. This gives the following Poisson equation

$$\nabla\cdot\left(\frac{1}{\rho^{n}}\nabla p\right)=\frac{1}{\Delta t}\left(\nabla\cdot u^{*}+\frac{J}{(\rho_{l}-\rho_{g})}\delta_{I}\right) \tag{9}$$

where δ_I is the Dirac distribution function expressing the fact that we added the source term coming from the evaporation flux $\mathbf{J}$ which is concentrated only in cells containing the interface. From Equation (3), the order of magnitude of $\mathbf{J}$ scales as $D_v(c_s-c_\infty)/r_0\sim 10^{-4}$. Then, from Equation (9), we found than the added source term is negligible and does not matter for interface dynamics, in our case considering a pure diffusive model. Nevertheless, for the understanding of the vapor dynamics outside of the droplet, this added source term is necessary because the low vapor density compared to the liquid density does pushed the

saturated vapor from the interface giving a Stefan flow. Finally, the $n+1$ velocity field is computed as

$$\boldsymbol{u}^{n+1} = \boldsymbol{u}^{*} - \Delta t \frac{1}{\rho^{n}} \nabla p \tag{10}$$

3.3. Diffusion equation

For the interface advection, we have to solve in a first time the diffusion equation given by Equation (1). We use a time-implicit backward Euler discretisation, then we write the vapor concentration c at the time step $n+1$ as

$$c^{n+1} = c^{n} + \Delta t \nabla \cdot (D_v \nabla c^{n+1}) \tag{11}$$

This leads to a Poisson-Helmholtz problem for c^{n+1} with the following boundary conditions: the saturation vapor c_s at the interface and the vapor value at the computational domain limits at given relative humitidy H, $c_\infty = H c_s$. The system of equations resulting is solved using a multigrid solver.

3.4. Advection of the interface

For the evaporating droplet dynamics, the interface needs to be tracked and followed. Therefore, once the velocity field is computed, a Volume-Of-Fluid (VOF) method is used [29]. The VOF approach enables a satisfactory reconstruction of the interface and guarantees the mass conservation using a conservative advection transport. The VOF method consists into two steps:

1. from the volume fraction f, we localize the cells that contain parts of the interface and we reconstruct the interface shape piece by piece with an affine function.
2. we advect the interface with a velocity field corresponding to the outward evaporation mass flux. This flux is calculated for each time step according Equation (2) once the vapor concentration, c, is computed by Equation (11).

In our model, the flux gives an "evaporation velocity" or an "interface velocity" which leads to the interface displacement. It does not correspond to the velocity

of fluid particles, it is the result of the loss for each time step of a small slice of liquid replaced by some vapor. The "evaporation velocity" is added to the mixed cells containing the interface, as described by Equation 9.

3.5. Contact angle implementation

For the sessile droplet configuration, the droplet is deposited on a substrate made of a non-corrosive material. We modelled the action of the substrate on the droplet by setting the value of the contact angle, θ, defined as the angle between the drop interface and the solid surface. Changing the contact angle is equivalent to changing the material type of the substrate, for instance, a water droplet on a silver substrate can form a contact angle close to 90°, which is a particular case of interest, whereas on gold substrates smaller contact angles around 30° are mesured [30]. These values depend on the surface condition of the material and they can also be influenced by the droplet size [31]. The contact angle can vary or not during the evaporation process, the different cases will be discussed in Section 4. Before presenting the numerical results of the two modes, we need to describe the implementation of the contact angle and the pinned interface in the framework of the VOF reconstruction.

For the contact angle, we followed the method of Afkhami et al. [32]. In a 2D case, the cell containing the triple contact point is marked as a cell along the solid boundary with a volume fraction $f \neq 0$ and $f \neq 1$ and with a right cell with $f = 0$. This defines without ambiguity the cell. We compute the height functions for the two cells above the substrate (lines $h[1]$ and $h[2]$ in the Figure 3) in the horizontal direction from the y axis. We need some extra points to compute the curvature correctly at the triple point. We extend the work of [32] to a 5x5 stencil: consequently, the values of the ghost cells at each time step (two layers below the substrate, $h[-1]$ and $h[-2]$) are extrapolated linearly from the layers 1 and 2 above the substrate to impose a given contact angle

$$h[-1] = h[1] + \Delta / \tan\theta \tag{12}$$

where Δ denotes the cell size. $h[-2]$ is computed in the same way. We note that

for $\theta < 45^\circ$, we would compute the height function by the signed distance to the x axis. It is known that horizontal signed functions are more complicated to define accurately: anyway, the approach works fine enough with small angles.

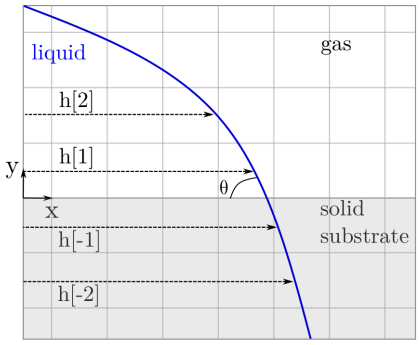

Figure 3: Use of horizontal height functions for the imposed contact angle θ. The height functions $h[1]$ and $h[2]$ allow to extrapolate the values of the ghost cells $h[-1]$ and $h[-2]$ which are then used to compute the curvature at the triple contact point and deduce the contact angle.

The classical VOF approach uses staggered grids for the velocity field then the normal and tangential components of the velocity at the substrate boundary ($y = 0$) are equal to zero by imposing the ghost cell values of the layers below the substrate. A consequence is that implementing an interface pinned configuration is quite complicated, the reason is that in the VOF approach the volume fraction f is transported with the staggered velocity field $\mathbf{u}$ resulting from the solution at time t of the Navier-Stokes equations using $\partial_t f + \nabla \cdot (f\mathbf{u}) = 0$. The staggered velocity field $\mathbf{u}$ over the 1st cell above the substrate has nonnul horizontal components u_x (for a cell of size Δ, the horizontal components are placed at $\Delta/2$) given a numerical slip when the volume fractions are transported, hence it is very difficult to assure the stability of the pinned point of the interface at the boundary condition. Refining the numerical grid helps as the numerical slip scales with Δ. Hooking a fixed point on a boundary condition needs precise handling: in the novel pinned implementation we have to modify the VOF reconstruction step to take into account specifically the conditions of constant radius and decreasing contact angle θ as a function of time

. Figure 4 presents three schematics of a boundary cell containing the triple

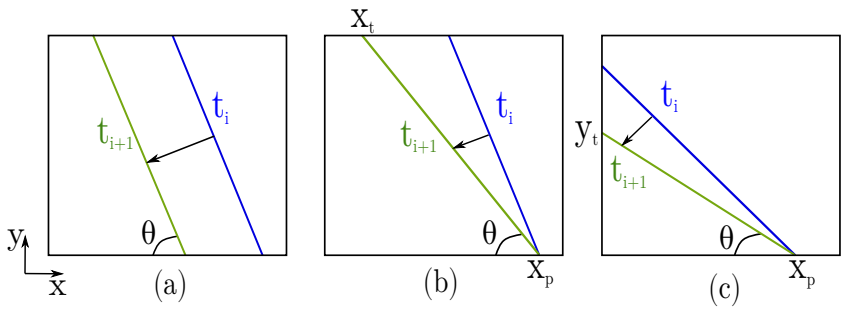

Figure 4: Schematics of the two steps VOF reconstruction on a boundary cell with a triple contact line: (a) is the classical reconstruction where the droplet radius decreases while evaporating always at constant contact angle θ, (b) and (c) are two cases of the new pinned mode depending of the line intersection, where the droplet radius is constant and the contact angle θ decreases as a function of time.

point (the bottom side represents the substrate): on the left, the classical VOF reconstruction for an unpinned evaporation mode and in the middle and on the right, the new pinned reconstruction. Figure 4 (a) shows the slipping of the interface along the substrate with a contact angle θ which remains constant. For the novel pinned reconstruction approach, we proceed as following: once we compute the volume fraction at the next time step, $f(t_1)$ with $t_1 = t + dt$, we determine geometrically the new angle θ which keeps the mass in the local cell. This is done by defining the piecewise segment of the interface reconstruction passing through the pinned point x_p. In the following for sake of simplicity, we explain the algorithm in a local cartesian basis. The axisymmetrical equivalent is straightforward. The algorithm is composed of two different cases depending on the intersection point of the reconstructed piecewise segment with the cell boundaries. First, we normalize the distance with the cell size Δ, a dynamical variable depending on the time and space but fixed for a given time step. Secondly, we scale the value x_p using a local basis, in which the origin is placed at the left bottom corner of the cell, therefore we have all the lengths in the range $[0, 1]$ and Δ becomes equal to one. We have then:

1. the reconstructed segment passing through the pinned point x_p crossing

the top of the cell at the point x_t (Figure 4 (b)), then we have to compute the surface by a trapeze formule $f(t_1) = (x_p + x_t)/2$ to find x_t. We have finally: $\tan\theta_{i+1} = 1/(x_p - x_t)$.

2. if the reconstructed segment passing through the pinned point x_p crosses first the left side of the cell at the point y_t (Figure 4 (c)) we use a triangle formula $f(t_1) = y_t x_p/2$ for the surface and we have simply: $\tan\theta_{i+1} = 2\ f(t_1)/x_p^2$.

Once the angle θ_{i+1} of the pinned interface is computed we use the contact angle procedure to impose the boundary condition at the substrate, then θ_i is set to θ_{i+1} at each iteration.

4. Results and discussion

The system is an evaporating droplet of liquid surrounded by air. Both phases have spatially uniform and constant density and viscosity. The entire system is at ambient temperature during the simulation. Temperature gradients are neglected and assuming a constant and controlled temperature during the whole simulation appears coherent with experiments [6]. The surface tension of the liquid-gas interface γ and the temperature are assumed uniform and constant, as a pure liquid is considered in this study. For the vapor, we have to verify the following conditions: (i) on the interface of the droplet, the vapor concentration is the saturated vapor concentration c_s and (ii) far away from the interface, the vapor concentration is fixed to c_∞. For a sessile droplet, we need to add the following conditions: (iii) the vapor concentration gradient normal to the substrate is zero because there is no vapor flux and (iv) the fluid does not penetrate the solid substrate, then $\mathbf{u}\cdot\mathbf{n} = 0$. For all simulations, we assume that at $t = 0$, the drop is in an equilibrium shape and that the velocity field is set to zero. The dimensionless parameters used in the simulations are: $R_0 = 1$, $Pe = 10^{-3}$, $c_s = 1$ and c_∞ ranges from 0 to 1 depending on the relative humidity needed. In order to recover the dimensionalized results, the numerical results have to be multiplied by the time and the space scales.

4.1. Validation: spherical droplet in still air

We first test our model on a simpler case, a spherical droplet motionless in an infinite uniform medium considering the quasi-steady regime hypothesis [33]. Based on the Equation (2) for the outward evaporation mass flux and recalling that $dm = 4\rho_l \pi r_0^2 dr$, we can obtain as solution the well-known squared radius relation, the d^2 law

$$r_0^2 - r^2(t) = 2\frac{D_v\,(c_s - c_\infty)}{\rho_l}t \tag{13}$$

The d^2 law is valid for an infinite medium, but the numerical domain has a finite size, L, where the droplet of size r_0 is placed. A parametric study showed that, for $L \sim 10r_0$, the finite size L does not affect significatively the results for the vapor concentration distribution and consequently for the global evaporation of the droplet. As shown on Figure 5, we obtain a good agreement between our numerical results and the analytical law.

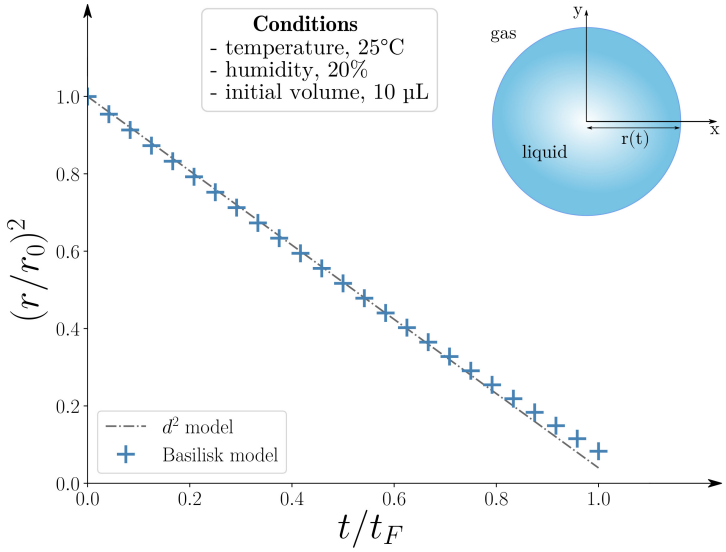

Figure 5: Validation case with a spherical droplet. The numerical results $(r/r_0)^2$ are plotted (crosses) and compared with the analytical d^2 law (dashed dotted line).

4.2. Unpinned case

The unpinned mode of evaporation appears for droplets of pure liquid on perfectly smooth surfaces. The mode parameters of the simulations were chosen to reproduce the evaporation of a pure water sessile droplet on silicon wafers. At $t = 0$, the droplet is in an equilibrium position and forms a spherical cap with a contact angle θ as illustrated on Figure 6: the contact radius decrease in time while the contact angle remains constant.

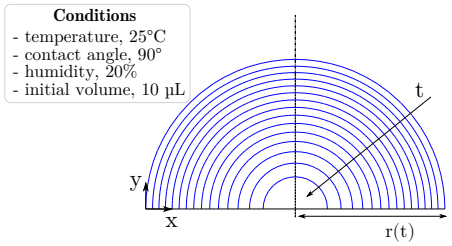

Figure 6: Interface reconstructed numerically for the unpinned mode during evaporation. The interface (in blue) slices on the solid substrate (in black), with a constant contact angle as the time t evolves.

The case presented here represents a sessile droplet with $\theta = 90^\circ$, a half-sphere, which is a particular case identical to the case of the spherical droplet in air and follows the d^2 law from Equation (13). We study the evolution in time of the droplet volume (V/V_0) for different contact angles between 0 and 90° and different relative humidities between 0 and 80%, using the Equation (5). Figure 7 presents the results of the parametric study realized to analyze the influence of the relative humidity on the evaporation behaviour, for the particular case of a half-sphere. We observe that the volume evolves like $t^{3/2}$ as the evolution of $(V/V_0)^{2/3}$ as function of (t/t_F) is linear for all the different relative humidities tested. This is coherent with the d^2 law and quite expected with this case where $\theta = 90^\circ$. Besides, the inset in Figure 7 shows that the evaporation rate decreases linearly as the relative humidity increases as expected by comparison with the analytical work of [9].

Figure 8 shows that sessile droplets with contact angles between 90° and 45°

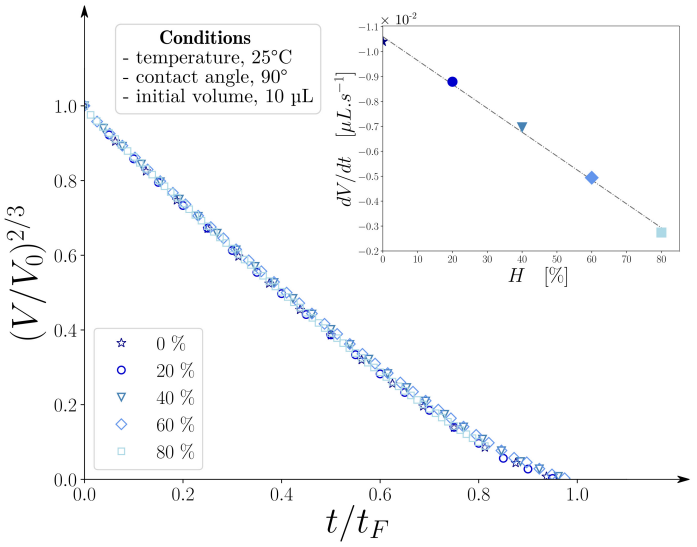

Figure 7: Numerical study on the influence of the relative humidity on evaporation in the unpinned mode. The simulations were all performed with a pure liquid sessile droplet of $10\mu L$ forming a contact angle of 90°. The normalized volume is plotted as a function of the scaled time. The inset shows the variation of the evaporation rate as a function of the relative humidity.

follow the same typical evaporation profile. The volume evolves again like $t^{3/2}$, which means that the d^2 law (Equation 13) can be generalized to sessile droplets with contact angles below $\theta = 90^\circ$. An accurate measure of the contact angle can be hard to achieve especially under 50° which explains that some points do not fit perfectly. The evaporation rate decreases linearly as contact angle increases which is coherent with the analytical relation of [9].

Considering these results in addition to litterature [34, 9], we can conclude that the relative humidity does not influence the general form of the droplet volume-versus-time curve. But changing the relative humidity influences of course the total time of evaporation. Finally, we can be established that, without regard to geometrical parameters, pure liquid sessile droplets evaporate in the unpinned mode following the same behaviour, which can be described by a general d^2 law.

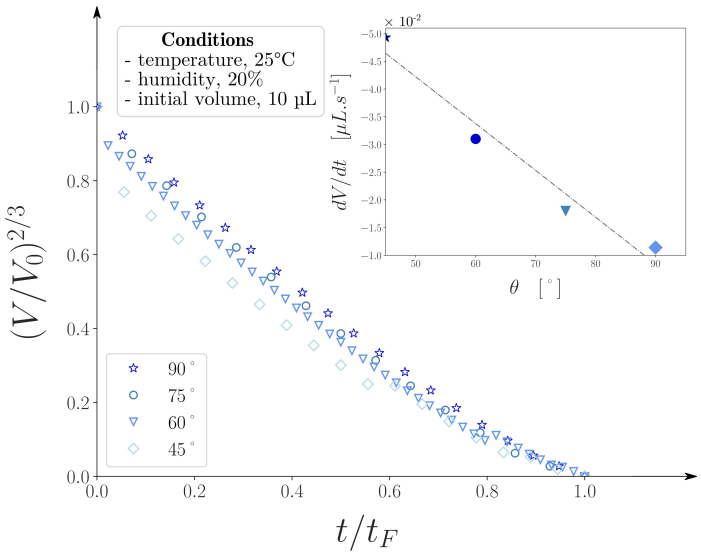

Figure 8: Numerical study on the influence of the contact angle on evaporation in the unpinned mode.The simulations were all performed with a pure liquid sessile droplet of $10\mu L$ forming a contact angle of 90°. The normalized volume is plotted as a function of the scaled time. The inset shows the variation of the evaporation rate as a function of the contact angle.

4.3. Pinned case

The pinned mode usually appears for drops containing particles or when the substrate is rough. In our simulations, we want to reproduce the evaporation of a pure water droplet where the interface is pinned due to surface roughness. This work will be then extended to cases where the pinning results from the accumulation of particles at the anchorage point.

To validate our numerical data for the pinned mode, we did experiments in an airtight glove box of 250 L under hygrometry and temperature control. The relative humidity, H, can range from 5% and 50% and remains constant during the whole experiment ($\pm 2\%$). In each experiment, a droplet of 10μL of distilled water is deposited onto a substrate with a micropipette. Both liquid and substrate are at room temperature, $T = 25 \pm 2^\circ$ C at the initial state. The temperature is continuously measured in the box and can be considered constant. A rough copper substrate is used to obtain the pinned mode. The height, the radius,

and the contact angle of the sessile droplet are measured using a Nikon D810 camera with a Navitar lens recording an image every 30 secondes from the side. The experimental data are presented on Figure 10.

In the pinned mode, the interface of the droplet is pinned to the substrate during the evaporation. The contact area and thus the contact radius r are constant in time whereas the contact angle θ decreases: this ensures that the drop keeps a spherical-cap shape as illustrated in Figure 9.

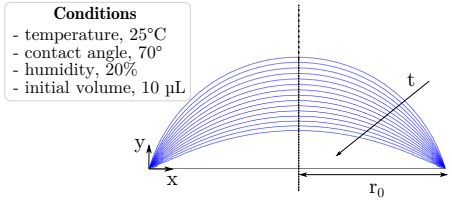

Figure 9: Interface reconstructed numerically for the pinned mode during evaporation. The interface (in blue) is pinned to the solid substrate (in black) while the contact angle decreases, as the time t evolves.

As for the unpinned case, we calculate the volume evolution in time, using the Equation (5). Figure 10 presents the numerical results compared with the experimental data for a sessile droplet with an initial contact angle $\theta = 70^\circ$. We observe that the non-dimensionalized volume (V/V_0) varies linearly with the time (t/t_F). When the contact angle becomes small (under 20°), the reconstruction of the interface and the measure of the contact angle are not well captured by our implementation: the numerical error increases as the droplet interface is almost horizontal and the calculation with the height functions should be improved to obtain more accurate results. The experimental data validate the numerical model for the pinned evaporation mode.

This means that the d^2 is not valid anymore in this case. To explain the linear dependancy of the volume in time, we can perform a Taylor expansion of Equation (5). This shows that the volume evolution can be considered linear with the contact angle which is coherent with the following theoretical law [14]

$$\theta(t) = \theta_0(1 - t/t_F) \tag{14}$$

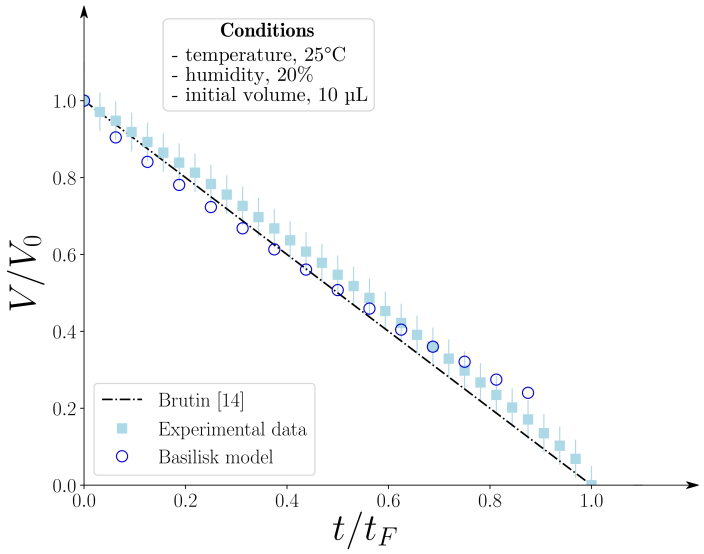

Figure 10: Normalized droplet volume as function of the scaled time for the pinned evaporation mode. Numerical results (circles) are compared with our experimental data (filled squares) and with a theoretical law (dashed dotted line).

This is also coherent with the experimental results presented in [23] or [34] and the numerical results of [24].

5. Conclusions

We presented a numerical approach to simulate the evaporation behaviour of pure liquid sessile droplets as a first step toward the study of mixtures evaporation. To validate the numerical approach we proposed to analyse two academic configurations: the unpinned mode where the contact angle is constant and the pinned mode where the wetting area is constant.

The numerical results show that the evaporation model gives accurate results for both modes when there are compared to analytical solutions and experimental data. For the unpinned mode, we conclude that irrespective of the geometrical parameters of sessile droplets, sessile droplets containing a pure liquid evaporates following the same behaviour described by a general d^2 law. For

the pinned case, we developed a new algorithm for the contact angle implementation in the framework of the VOF reconstruction which allows to impose a boundary condition at the substrate and then adapt the contact angle. The confrontation with experiments and theoretical law is very satisfactory although the proposed approach presents some limits for contact angles below 20 $^\circ$ due to the interface reconstruction inherent to the VOF. Using a mixed height function approach for smalls contact angles could be an interesting option. This contact angle implementation in the pinned case now allows to analyse more complex problems, as mixture droplets and in particular saline sessile droplets, when Marangoni gradients of the surface tension and saline transport have to be taken into account in the numerical model. The pinning of the drop will have to consider the concentration of particles near the triple contact line, modifying in particular the Raoult's law in the numerical model.

References

[1] J. C. Maxwell, Collected Scientific Papers. Vol. 2, CUP, 1890.

[2] I. Langmuir, The evaporation of small spheres, Physical review 12 (5) (1918) 368.

[3] R. D. Deegan, O. Bakajin, T. F. Dupont, G. Huber, S. R. Nagel, T. A. Witten, Capillary flow as the cause of ring stains from dried liquid drops, Nature 389 (6653) (1997) 827–829.

[4] Y. O. Popov, Evaporative deposition patterns: spatial dimensions of the deposit, Physical Review E 71 (3) (2005) 036313.

[5] H. Y. Erbil, Control of stain geometry by drop evaporation of surfactant containing dispersions, Advances in colloid and interface science 222 (2015) 275–290.

[6] V. Soulié, S. Karpitschka, F. Lequien, P. Prené, T. Zemb, H. Moehwald, H. Riegler, The evaporation behavior of sessile droplets from aqueous saline

solutions, Physical Chemistry Chemical Physics 17 (34) (2015) 22296–22303.

[7] J. Park, J. Moon, Control of colloidal particle deposit patterns within picoliter droplets ejected by ink-jet printing, Langmuir 22 (8) (2006) 3506–3513.

[8] M. Kuang, L. Wang, Y. Song, Controllable printing droplets for high-resolution patterns, Advanced materials 26 (40) (2014) 6950–6958.

[9] R. Picknett, R. Bexon, The evaporation of sessile or pendant drops in still air, Journal of Colloid and Interface Science 61 (2) (1977) 336–350.

[10] S. M. Rowan, M. Newton, G. McHale, Evaporation of microdroplets and the wetting of solid surfaces, The journal of physical chemistry 99 (35) (1995) 13268–13271.

[11] C. Bourges-Monnier, M. Shanahan, Influence of evaporation on contact angle, Langmuir 11 (7) (1995) 2820–2829.

[12] J. Eggers, L. Pismen, Nonlocal description of evaporating drops, Physics of Fluids 22 (11) (2010) 112101.

[13] G. Dunn, S. Wilson, B. Duffy, S. David, K. Sefiane, A mathematical model for the evaporation of a thin sessile liquid droplet: Comparison between experiment and theory, Colloids and Surfaces A: Physicochemical and Engineering Aspects 323 (1-3) (2008) 50–55.

[14] D. Brutin, Droplet wetting and evaporation: from pure to complex fluids, Academic Press, 2015.

[15] L. Scriven, C. Sternling, The marangoni effects, Nature 187 (4733) (1960) 186–188.

[16] E. Bormashenko, Y. Bormashenko, R. Pogreb, O. Stanevsky, G. Whyman, Droplet behavior on flat and textured surfaces: Co-occurrence of deegan outward flow with marangoni solute instability, Journal of colloid and interface science 306 (1) (2007) 128–132.

[17] M. Majumder, C. S. Rendall, J. A. Eukel, J. Y. Wang, N. Behabtu, C. L. Pint, T.-Y. Liu, A. W. Orbaek, F. Mirri, J. Nam, et al., Overcoming the "coffee-stain" effect by compositional marangoni-flow-assisted drop-drying, The Journal of Physical Chemistry B 116 (22) (2012) 6536–6542.

[18] T. Still, P. J. Yunker, A. G. Yodh, Surfactant-induced marangoni eddies alter the coffee-rings of evaporating colloidal drops, Langmuir 28 (11) (2012) 4984–4988.

[19] H. Hu, R. G. Larson, Evaporation of a sessile droplet on a substrate, The Journal of Physical Chemistry B 106 (6) (2002) 1334–1344.

[20] S. Popinet, http://basilisk.fr.

[21] M. Renardy, Y. Renardy, J. Li, Numerical simulation of moving contact line problems using a volume-of-fluid method, Journal of Computational Physics 171 (1) (2001) 243–263.

[22] P. D. Spelt, A level-set approach for simulations of flows with multiple moving contact lines with hysteresis, Journal of Computational physics 207 (2) (2005) 389–404.

[23] S. Narayanan, J. Wang, X.-M. Lin, Dynamical self-assembly of nanocrystal superlattices during colloidal droplet evaporation by in situ small angle x-ray scattering, Physical review letters 93 (13) (2004) 135503.

[24] L. Y. Barash, T. Bigioni, V. Vinokur, L. Shchur, Evaporation and fluid dynamics of a sessile drop of capillary size, Physical Review E 79 (4) (2009) 046301.

[25] R. D. Deegan, O. Bakajin, T. F. Dupont, G. Huber, S. R. Nagel, T. A. Witten, Contact line deposits in an evaporating drop, Physical review E 62 (1) (2000) 756.

[26] J. D. Jackson, Classical electrodynamics, John Wiley & Sons, 2007.

[27] S. Popinet, An accurate adaptive solver for surface-tension-driven interfacial flows, Journal of Computational Physics 228 (16) (2009) 5838–5866.

[28] S. Popinet, Numerical models of surface tension, Annual Review of Fluid Mechanics 50 (2018) 49–75.

[29] G. Tryggvason, R. Scardovelli, S. Zaleski, Direct numerical simulations of gas–liquid multiphase flows, Cambridge University Press, 2011.

[30] F. Bartell, P. H. Cardwell, Reproducible contact angles on reproducible metal surfaces. i. contact angles of water against silver and gold1, Journal of the American Chemical Society 64 (3) (1942) 494–497.

[31] R. J. Good, M. Koo, The effect of drop size on contact angle, Journal of Colloid and Interface Science 71 (2) (1979) 283–292.

[32] S. Afkhami, M. Bussmann, Height functions for applying contact angles to 2d vof simulations, International journal for numerical methods in fluids 57 (4) (2008) 453–472.

[33] Q. Magdelaine, Hydrodynamique des films liquides hétérogènes, Ph.D. thesis (2019).

[34] V. Soulié, Sessile droplets of salt solutions on inert and metallic surfaces: Influence of salt concentration gradients on evaporation and corrosion behaviour, Ph.D. thesis (2015).